Optik - International Journal for Light and Electron Optics 224 (2020) 165716

Contents lists available at ScienceDirect

Optik

journal homepage: www.elsevier.com/locate/ijleo

Original research article

Fast hyperspectral imager driven by a low-cost and compact galvo-mirror

Xiaomei Liu [a], Ziqi Jiang [a], Tianci Wang [a], Fuhong Cai [a,b,*], Dan Wang [c,**]

[a] Mechanical and Electrical Engineering College, Hainan University, Haikou, Hainan, 570228, China
[b] School of Biomedical Engineering, Hainan University, Haikou, Hainan, 570228, China
[c] State Key Laboratory of Organic-Inorganic Composites, Beijing University of Chemical Technology, Beijing, 100029, China

ARTICLE INFO

Keywords:
Galvo-mirror scanning
Imaging spectrometer
High speed

ABSTRACT

Imaging spectrometer is a critical device for remote sensing in visible and infrared band. Nowadays, it has become a powerful instrument to obtain three-dimensional hyperspectral cube (two-dimensional spatial information and one-dimensional spectral information) of targets for high precision object recognition. However, we often cannot meet the requirements of high spatial resolution and high spectral resolution at the same time. So there is still a trade-off between detection speed and data accuracy (including spatial and spectral resolution). In this paper, we developed a fast and high spectral resolution imaging spectrometer to obtain the spectral-spatial information with the help of a low-cost and compact galvo-mirror. The spectrometer has a wavelength resolution of about 10 nm at visible-near infrared band (400 nm–800 nm), and it can measure two-dimensional spatial images of various biological samples (including corals, dragon fruits and human hands) at various wavelengths repeatedly. This spectrometer can facilitate collection of a large number of spectral image data during half cycle of galvo-mirror scanning. The theoretical acquisition speed of hyperspectral cube can reach more than 1 MHz. However, at this acquisition speed, the signal-to-noise ratio of the camera is poor, and it is unable to obtain high-quality signals. We believe that with the improvement of camera performance, our prototype can obtain hyperspectral data at a higher sampling speed.

1. Introduction

The utilization of imaging spectroscopy is one of the most important developments in the field of remote sensing. Imaging spectrometers have the advantages of high spectral resolution and the combination of images and spectra [1,2]. Therefore, they are used in the screening and surveillance of material components in objects of interest. The characteristic of spectral imaging is that two-dimensional spatial information and one-dimensional spectral information of the detected object can be obtained at the same time, and this technology also has the advantage of non-destructive testing. This makes imaging spectrometers widely used in modern scientific experiments, including biological research [3–6], food monitoring [7–9], agricultural production [10,11] and other fields. As a high-resolution imaging spectroscopy technology, it is able to support us find and identify various lesions in a non-contact manner. This technique has been successfully applied in brain surgery [12,13]. At the same time, the combination of hyperspectral imager and

* Corresponding author at: Mechanical and Electrical Engineering College, Hainan University, Haikou, Hainan, 570228, China.
** Corresponding author.
E-mail addresses: caifuhong@zju.edu.cn (F. Cai), wangdan@mail.buct.edu.cn (D. Wang).

https://doi.org/10.1016/j.ijleo.2020.165716
Received 29 June 2020; Accepted 28 September 2020
Available online 2 October 2020

endoscopy has also attracted wide attention. Hyperspectral endoscopy has been developed and has the possibility of clinical applications [14–16]. In terms of food safety control, imaging spectroscopy also plays an important role to help us judge the quality of food. Yao et al. developed a hand-held imaging spectrometer to realize pH non-destructive detection of pork [17]. Meanwhile, hyperspectral imaging can also be used to non-destructively evaluate fruit quality accurately [18,19]. In archeology and arts protection, Wu et al. found that the SWIR imaging spectrum technology can not only help us to extract the line features in the painting, but also to identify the colors in the painting [20].

There are three scanning modes of hyperspectral camera: i. push-broom scan [21], ii. snapshot [22] and iii. adjustable filter [23]. Nowadays, rotational scanning imaging spectroscopy has also been developed for staring spectral imaging, but this technology is not mature enough [24,25]. The mainstream imaging spectrometer system uses push-broom scan mode. However, the acquisition speed of hyperspectral cube with push-broom scanning imaging spectrometer is relatively slow, and it usually takes more than a few seconds to complete a hyperspectral scan. For example, in brain surgery, hyperspectral imaging system can be used to carry out surgical navigation [26]. But its imaging speed is low, so it can't realize real-time monitoring. In our work, the push-broom module of an imaging spectrometer was replaced with a galvo-mirror for spatial scanning to obtain the spectral cubes of the objects of interest. While the scanning period of the galvo-mirror is short, this method enables us to obtain more information of the target quickly. For the current prototype, the spectral resolution of the imaging spectrometer is about 10 nm, and the spectral range is 400 nm–800 nm. With this galvo-mirror scanning spectrometer, we performed optical inspection of coral, dragon fruit, and human hand. During the scanning experiments, the brightness of LED light source is about 500 lumens. Based on the experimental spectral results, we can test the maturity of dragon fruit and monitor the hemoglobin in human hand. In addition, through the galvo-mirror scanning imaging spectrometer, the acquisition speed of hyperspectral cube can reach 1 cube/s. With better lighting conditions and camera performance, the imaging speed can be further improved.

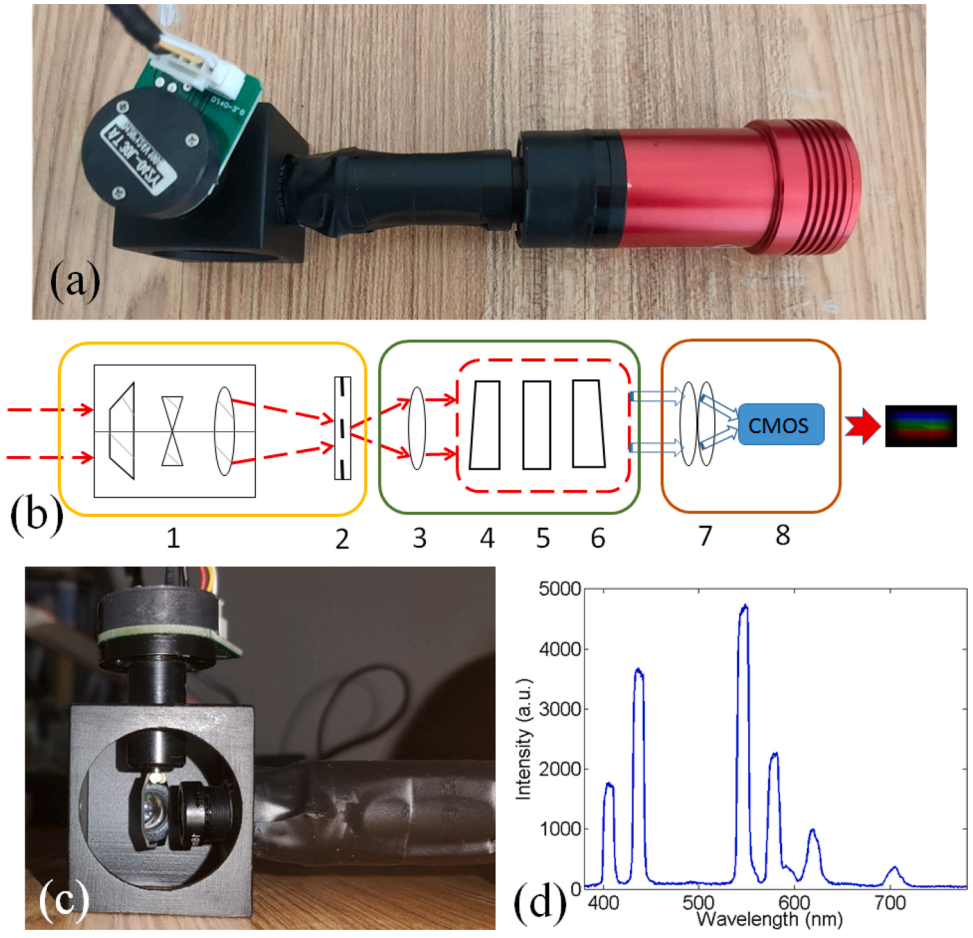

Fig. 1. (a) Photo of our imaging spectrometer. (b) Schematic illustration of the imaging spectrometer. A classic prism-grating-prism setup was selected to build the imaging spectrometer, whose optical elements: (1) imaging lens; (2) slit; (3) doublet lens; (4) prism; (5) grating; (6) prism; (7) project lens; (8) CMOS camera. (c) Installation photo of galvo-mirror, which was as close to the imaging lens as possible. (d) A spectrum of mercury lamp obtained by our imaging spectrometer.

2. Methods and materials

The photo of our galvanometer scanning imaging spectrometer system was shown in Fig. 1(a), and a classic prism-grating-prism setup was selected as the imaging spectrometer [27] (shown in Fig.1(b)), which consists of an imaging module, a diffraction module, and a detection module. Specifically, the spectrometer is made up of inexpensive off-the-shelf optical elements and the use of transmission grating modules ensures good imaging quality and compact size. Except for the galvo-mirror, the other optical elements have regular shapes and can be installed in a metal tube. These optical elements can be clamped by two stationary rings (SM05RR, Thorlabs, Newton, New Jersey, USA). In our work, we used the slotted tube SM05L20C to install the doublet lens (3), prism (4, 6) and grating (5). These (SM05RR and SM05L20C) could be connected via a mechanical thread. We could rotate the SM05RR to adjust the slit orientation. A closed-circuit television imaging (CCTV) lens (1, f =12 mm), whose diameter is about 12 mm, was selected to capture the external light. This imaging lens was installed at the front of the SM05L20C. When the imaging spectrometer was utilized to detect object, the light (e.g. fluorescence; or reflected) emitted from a line area of an object entered the system through the imaging lens (1). The light then projected the image onto the slit (2). A doublet lens (3) collimated the light passing through the slit. Then we used a prism grating prism module (4–6, 300 lines / mm grating) to extend the spectrum to the detection module. The galvo-mirror was installed before the imaging lens, as shown in Fig.1(c). A mercury lamp was utilized as a calibrate Light and its detected spectrum was shown in Fig.1(d), which was consistent with the results of commercial spectrometers [28].

Next, the specific method of galvo-mirror scanning is explained. In high-end laser scanning microscope such as confocal and two-photon, galvo-mirror was widely used [29]. Hence its technology is very mature and its performance is very stable. The driving method of the galvo-mirror is simple and easy to use. The scanning angle of the galvo-mirror is proportional to the driving voltage signal, and the scanning rate can reach the magnitude of MHz, which is more than enough in the spectral scanning. It should be noted that, a silver mirror can be installed in the galvo mirror system to realize light reflection, and its reflection efficiency is more than 97 % in the band of 450 nm–2000 nm. Therefore, the loss of light intensity caused by galvo-mirror scanning can be ignored. Herein, a 30 kpps galvo-mirror was selected as the scanning module and its price was about $250.

During scanning, the galvo-mirror's rotational angle amplitude was set as 4°, and its working scanning speed is 0.5pps. As shown in Fig.1(c), the galvo mirror, which was mounted in a GCM001 cage, was controlled by a voltage signal generated by a multifunction electronic device (USB6008, NI). The rotation angle is proportional to the voltage signal. The galvo-mirror should be as close to the CCTV lens of the imaging spectrometer as possible, and it should be ensured that the mirror will not collide with the lens during scanning. The galvo-mirror can reflect the light from the detected object into imaging spectrometer. The CCTV lens connected to the output port of GCM001 was used to capture the reflected imaging rays and formed a real image on the slit. After the imaging light passed through the slit, it entered the imaging spectrometer and finally formed a spectral image on the CMOS sensor. When the angle of the galvo mirror changes, the real image scanned through a slit. In this way, we obtained the spectral images from all the pixels from

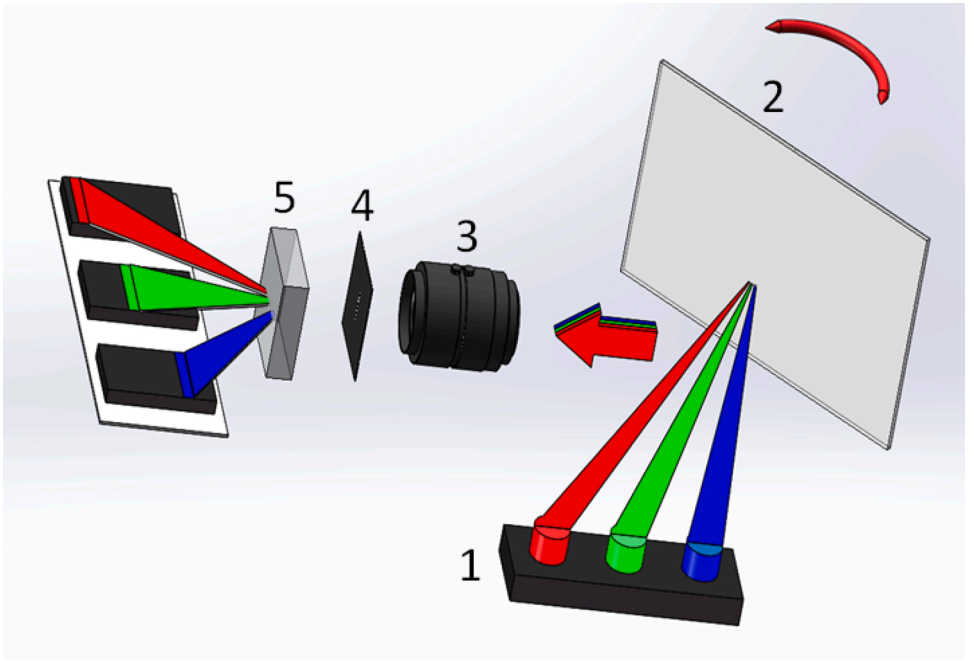

Fig. 2. Schematic illustration of galvo-mirror scanning imaging. 1. Objects of interest, 2. Galvo-mirror, 3. Imaging lens, 4. Slit, 5. Grating. With the scanning of galvo mirror, the lights of red object, green object and blue object pass through the optical axis of the imaging lens in turn, and enters the imaging spectrometer. (For interpretation of the references to colour in this figure legend, the reader is referred to the web version of this article).

the objects and the rapid scanning process was realized.

Fig. 2 showed the schematic diagram of galvo mirror scanning imaging. There are three objects in the spatial space, the colors of which were red, green and blue respectively. With the scanning of galvo mirror, the lights of red object, green object and blue object passed through the optical axis of the imaging lens in turn, and transmitted through the slit behind the imaging lens, and finally entered the camera CMOS ship. In this way, the high-speed scanning of spatial objects can be realized. In this scanning mode, we assumed that the light emitted by the object is approximately transmitted in parallel. This assumption is valid in the case of long-distance detection, but it cannot be applied for the micro range detection. Because optical remote sensing is usually used to monitor objects at a long distance, our system is suitable for remote sensing.

3. Results and discussion

In this section, we will introduce and discuss the experimental results from three galvo-mirror scanning experiments. Herein, human palm, coral and dragon fruit (pitaya) were selected as three samples respectively. Correspondingly, three hyperspectral cubes were obtained. The spatial intensity distributions extracted from the hyperspectral cubes were consistent with the morphology of the experimental samples, and the reflection spectra also reflected the characteristic molecular information of the corresponding region.

3.1. Scanning experiment for palm

As mentioned before, the hyperspectral imager can be applied to measure biological tissues. Herein, a hand (shown in Fig. 3(a)) was selected as the sample for galvo-mirror scanning imaging to verify the in vivo imaging potential of our system. The scanning time was one second in this experiment and a hyperspectral cube was obtained. Based on the hyperspectral cube, the reflection spatial intensity distribution of fingertips and palm was extracted and shown in Fig.3(b). The spectra of the finger and palm regions were also derived from the hyperspectral cube and shown in Fig.5(c) and (d), respectively. Because of the presence of blood, the colour of the hands is usually pale reddish. From a spectral point of view, this is because hemoglobin in blood will absorb light in the 400 nm–450 nm band and 550 nm – 600 nm band [30], which can also be found in Fig.5(c) and (d). Because the blood concentration of the palm was lower than that of the fingertip, the redness presented by the fingertip was deeper than the redness of the palm. So there was more hemoglobin in the fingertip. Since the finger's oxygen saturation is about 98 %, the main component of hemoglobin in fingers is oxyhemoglobin, whose spectral absorption peak is around 580 nm. Fig. 3(c) showed a absorption peak at 580 nm due to oxyhemoglobin. Because the blood concentration and oxygen saturation of palms were lower than those of fingers, the corresponding light absorption at 580 nm could not be observed clearly. It is worth noting that, this system can help us to monitor other parts of bio-tissue immediately without the need to contact the test object.

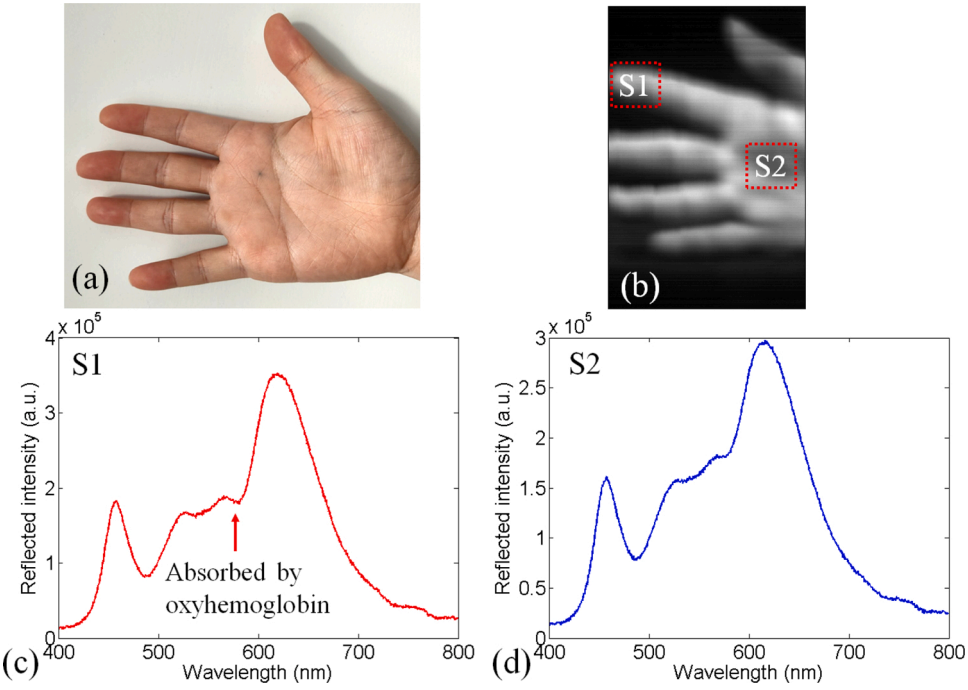

Fig. 3. The scanning results of the palm. (a). Photo of a human hand. (b) Spatial intensity distribution obtained from the scanning hyperspectral cube. (c) and (d) show the reflectance spectra from the fingertip and palm, respectively.

3.2. Scanning experiment for coral

To illustrate the performance of the imaging spectrometer, the spectra of coral was also investigated. The photo of the coral was shown in Fig. 4(a). The center of the coral was white and the surrounding of the coral was red. The chemical composition of corals was mainly $CaCO_3$ (calcium carbonate), which existed in the form of microcrystalline calcite aggregates. The cross section of coral has concentric circles and radial stripes, and its colour is white. Red is formed by corals absorbing about 1% of iron oxide in seawater during growth. The galvo-mirror imaging spectrometer was used to scan the coral to get hyperspectral cube. The scanning time was one second. The spatial image was shown in Fig.4(b). We can obtain the reflection spectra of each pixel through the hyperspectral cube. Among them, the spectra of the white region (marked as S1 region in Fig.4(b)) and the red region (marked as S2 region in Fig.4(b)) were shown in Fig.4(c) and (d), respectively. Obviously, the reflection spectrum of white area was more abundant. For example, in the 400 nm–500 nm band and 500 nm–600 nm band, the reflection spectrum from the white region was stronger than that from the red region. The reflection spectrum of red region was mainly concentrated in the band of 600 nm–700 nm. The intensity profiles of these two spectra were consistent with the colour characteristics of coral surface.

3.3. Scanning experiment for dragon fruit

Next, a dragon fruit was used as the sample for galvo-mirror scanning. The photo of the dragon fruit was shown in Fig.5 (a). The outer skin of the dragon fruit is the fruit peel. From flowering to fruit maturity, the colour of the peel gradually changes from green to red. As shown in Fig.5(a), For this ripe dragon fruit, only the marginal peel was green. The spatial image was shown in Fig. 5(b). The reflection spectrum of green fruit peel region (marked as S1 in Fig.5(b)) was shown in Fig.5(c). Observing this spectral waveform, There was a strong reflectivity in the green light band (500 nm – 600 nm), and an obvious light absorption appeared near 680 nm. This is because there was chlorophyll in the green fruit peel, which absorbed the red light. In the process of fruit ripening, chlorophyll was degraded. Therefore, in the reflection spectrum of red region (ripe fruit peel, marked as S2 in Fig.5(b)), there was no obvious absorption near 680 nm.

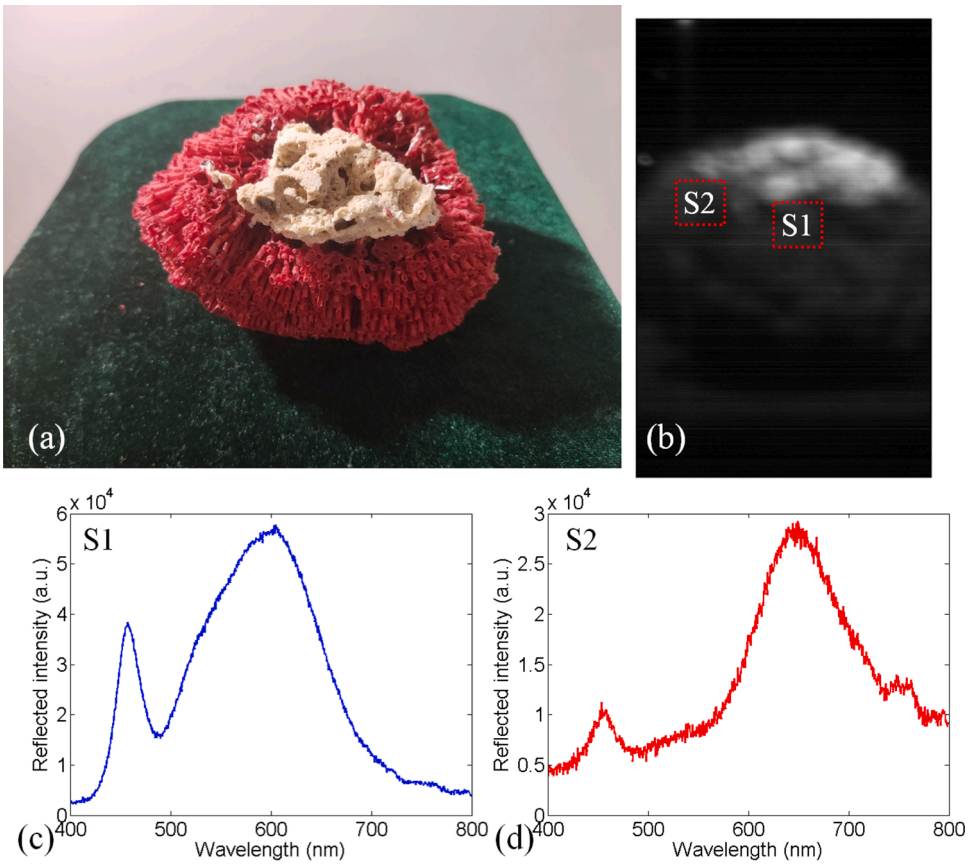

Fig. 4. The scanning results of the coral sample. (a). Photo of the coral sample. (b). Spatial intensity distribution obtained from the scanning hyperspectral cube. (c) and (d) show the reflectance spectra from the white region and the red region of the coral, respectively. (For interpretation of the references to colour in this figure legend, the reader is referred to the web version of this article).

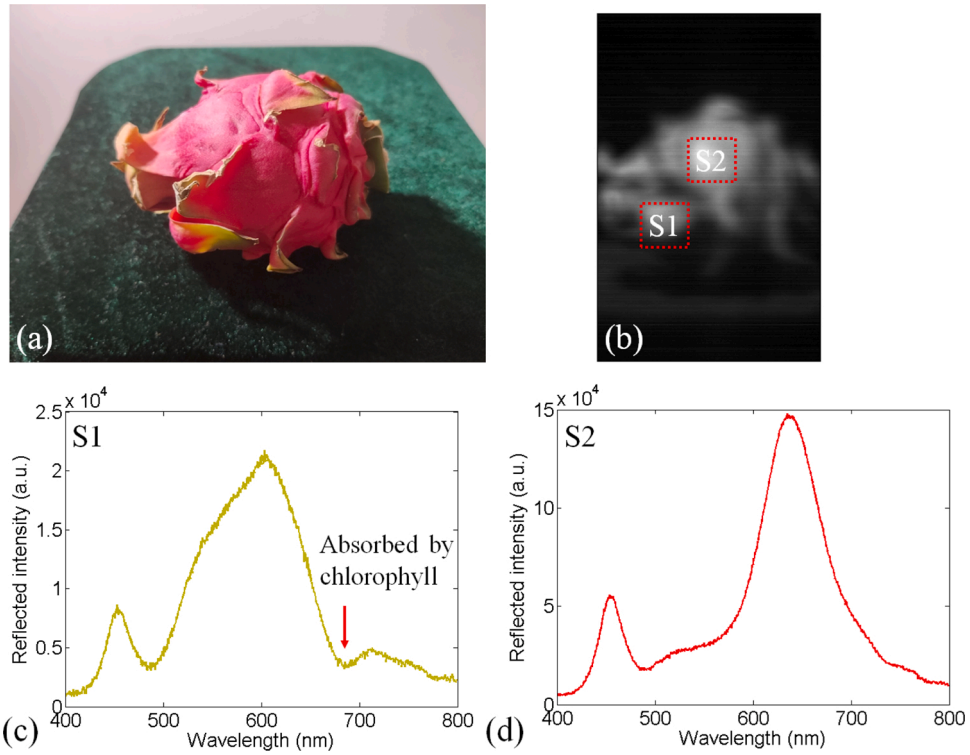

Fig. 5. The scanning results of the dragon fruit sample. (a). Photo of the dragon fruit sample. (b). Spatial intensity distribution obtained from the scanning hyperspectral cube. The spectra of the green and ripe fruit peel are shown in (c) and (d), respectively. (For interpretation of the references to colour in this figure legend, the reader is referred to the web version of this article).

4. Conclusion

Traditional imaging spectrometer usually needs to add relay imaging module, and use electromechanical stage to realize linear scanning of spatial dimension. We present a fast hyperspectral imager driven by a low-cost and compact galvo-mirror and verify its feasibility through experiments. The spectrometer has a wavelength resolution of about 10 nm at visible-near infrared band (400 nm–800 nm), and it can measure two-dimensional spatial images of various biological samples (including corals, dragon fruits and human hands) at various wavelengths repeatedly. Based our system, the hyperspectral cube of the detected object can be obtained in one second. During the experiments, the illumination intensity is about 500 lumens, and the camera we choose is an ordinary uncooled CMOS camera.

In our system, scanning galvo-mirror is installed in front of the imaging lens at the front end of the imaging spectrometer, and hyperspectral data is obtained through the angle scanning of galvanometer. The first advantage of this system is high cost performance. Scanning galvanometer is a kind of mature optical mechanical and electrical component, which only needs sawtooth voltage signal to drive it. Scanning speed is the second important advantage of scanning galvanometer. In the confocal / two-photon scanning imaging system, the scanning speed of galvanometer can reach 10^4 Hz-10^6 Hz. If the frame rate of the camera can reach 10^4 fps, our system can acquire one hyperspectral cube of a detected object with 1000 $\times$ 1000 pixels in 0.1 s. If we keep the spatial pixels unchanged and increase the frame rate of the camera, we can further improve the efficiency of hyperspectral acquisition. Therefore, our system has the potential to become a hyperspectral video recorder (about 24 cubes/second). At present, the frame rate of most mainstream cameras is about 100 fps. Therefore, the shortness that limits our system's acquisition efficiency mainly lies in the frame rate of camera. In the near future, we believe that with the improvement of camera performance, our prototype can obtain hyperspectral data with higher sampling speed for real-time hyperspectral monitoring.

Declaration of Competing Interest

None.

Acknowledgements

This research was funded by National Key Research and Development Program of China (2018YFC1407505); Hainan Provincial Natural Science Foundation of China (High level talent support project of basic and applied basic research plan, 2019RC080); the

scientific research fund of Hainan University (KYQD1653). Xiaomei Liu and Ziqi Jiang wrote the manuscript and performed the experiment; Tianci Wang processed the experimental data and revised the manuscript; Fuhong Cai and Dan Wang designed and built the hyperspectral imager.

References

[1] William L. Wolfe, Introduction to Imaging Spectrometers, Vol. 25, SPIE Press, 1997.
[2] Fuhong Cai, et al., Handheld four-dimensional optical sensor, Optik 203 (2020), 164001.
[3] Siqi Zhu, et al., Identification of cancerous gastric cells based on common features extracted from hyperspectral microscopic images, Biomed. Opt. Express 6 (4) (2015) 1135–1145.
[4] Chaojian Wang, et al., Multi-scale hyperspectral imaging of cervical neoplasia, Arch. Gynecol. Obstet. 293 (6) (2016) 1309–1317.
[5] Larisa A. Zherdeva, et al., In vivo hyperspectral imaging and differentiation of skin cancer, in: Optics in Health Care and Biomedical Optics VII, Vol. 10024, International Society for Optics and Photonics, 2016.
[6] Hamed Akbari, et al., "Hyperspectral imaging and quantitative analysis for prostate cancer detection.", J. Biomed. Opt. 17 (7) (2012), 076005.
[7] Jun Sun, et al., Research of moldy tea identification based on RF-RFE-Softmax model and hyperspectra, Optik 153 (2018) 156–163.
[8] Minto Michael, Randall K. Phebus, Jayendra Amamcharla, Hyperspectral imaging of common foodborne pathogens for rapid identification and differentiation, Food Sci. Nutr. 7 (8) (2019) 2716–2725.
[9] Ji Ma, et al., Advanced techniques for hyperspectral imaging in the food industry: principles and recent applications, Ann. Rev. Food Sci. Technol. 10 (2019) 197–220.
[10] Telmo Adão, et al., Hyperspectral imaging: a review on UAV-based sensors, data processing and applications for agriculture and forestry, Remote Sensing 9 (11) (2017), 1110.
[11] Pablo J. Zarco-Tejada, M.V. González-Dugo, E. Fereres, Seasonal stability of chlorophyll fluorescence quantified from airborne hyperspectral imagery as an indicator of net photosynthesis in the context of precision agriculture, Remote Sens. Environ. 179 (2016) 89–103.
[12] Himar Fabelo, et al., An intraoperative visualization system using hyperspectral imaging to aid in brain tumor delineation, Sensors 18 (2) (2018) 430.
[13] Himar Fabelo, et al., Deep learning-based framework for in vivo identification of glioblastoma tumor using hyperspectral images of human brain, Sensors 19 (4) (2019) 920.
[14] Jonghee Yoon, et al., A clinically translatable hyperspectral endoscopy (HySE) system for imaging the gastrointestinal tract, Nat. Commun. 10 (1) (2019) 1–13.
[15] Fuhong Cai, et al., Compact dual-channel (hyperspectral and video) endoscopy, Front. Phys. 8 (2020) 110.
[16] Swati S. More, James M. Beach, Robert Vince, Early detection of amyloidopathy in alzheimer's mice by hyperspectral endoscopy, Investigative ophthalmology & visual science 57 (7) (2016) 3231–3238.
[17] Xinli Yao, et al., Non-invasive and rapid pH monitoring for meat quality assessment using a low-cost portable hyperspectral scanner, Meat Sci. 152 (2019) 73–80.
[18] Yuan-Yuan Pu, et al., Ripeness classification of bananito fruit (Musa acuminata, AA): a comparison study of visible spectroscopy and hyperspectral imaging, Food Anal. Methods 12 (8) (2019) 1693–1704.
[19] Xiaoli Li, et al., SSC and pH for sweet assessment and maturity classification of harvested cherry fruit based on NIR hyperspectral imaging technology, Postharvest Biol. Technol. 143 (2018) 112–118.
[20] Taixia Wu, et al., Shortwave infrared imaging spectroscopy for analysis of ancient paintings, Appl. Spectrosc. 71 (5) (2016) 977.
[21] Samuel Ortega, et al., Hyperspectral push-broom microscope development and characterization, IEEE Access 7 (2019) 122473–122491.
[22] Ryan Priore, et al., Design of a miniature swir hyperspectral snapshot imager utilizing multivariate optical elements, in: Emerging Imaging and Sensing Technologies., Vol. 9992, International Society for Optics and Photonics, 2016.
[23] Konstantin B. Yushkov, Oleg Yu Makarov, Vladimir Ya Molchanov, Novel protocol of hyperspectral data acquisition by means of an acousto-optical tunable filter with synthesized transmission function, Opt. Lett. 44 (6) (2019) 1500–1503.
[24] Abdo Mohammad, Vlad Badilita, Jan Korvink, Spatial scanning hyperspectral imaging combining a rotating slit with a dove prism, Opt. Express 27 (15) (2019) 20290–20304.
[25] Fuhong Cai, et al., The design and implementation of portable rotational scanning imaging spectrometer, Opt. Commun. 459 (2020), 125016.
[26] Himar Fabelo, et al., Spatio-spectral classification of hyperspectral images for brain cancer detection during surgical operations, PLoS One 13 (3) (2018).
[27] Jianjun Chen, et al., Optical design of a short-wave infrared prism-grating imaging spectrometer, Appl. Opt. 57 (34) (2018) F8–F14.
[28] Fuhong Cai, et al., A mobile device-based imaging spectrometer for environmental monitoring by attaching a lightweight small module to a commercial digital camera, Sci. Rep. 7 (1) (2017) 1–9.
[29] Thomas A. Pologruto, Bernardo L. Sabatini, Karel Svoboda, ScanImage: flexible software for operating laser scanning microscopes, Biomed. Eng. Online 2 (1) (2003) 13.
[30] Perry Edwards, et al., Smartphone based optical spectrometer for diffusive reflectance spectroscopic measurement of hemoglobin, Sci. Rep. 7 (1) (2017) 1–7.